Quaternary Geochronology 19 (2014) 14–26

Contents lists available at SciVerse ScienceDirect

Quaternary Geochronology

journal homepage: www.elsevier.com/locate/quageo

Research paper

Chronology of Lateglacial ice flow reorganization and deglaciation in the Gotthard Pass area, Central Swiss Alps, based on cosmogenic ^{10}Be and *in situ* ^{14}C

K. Hippe [a,b,*], S. Ivy-Ochs [b], F. Kober [c], J. Zasadni [d], R. Wieler [a], L. Wacker [b], P.W. Kubik [b], C. Schlüchter [e]

[a] Institute of Geochemistry and Petrology, ETH Zürich, Clausiusstrasse 25, CH-8092 Zürich, Switzerland
[b] Laboratory of Ion Beam Physics, ETH Zürich, Schafmattstrasse 20, CH-8093 Zürich, Switzerland
[c] Geological Institute, ETH Zürich, Sonneggstrasse 5, CH-8092 Zürich, Switzerland
[d] AGH University of Science and Technology, Faculty of Geology, Geophysics and Environmental Protection, Al. Mickiewicza 30, 30-059 Kraków, Poland
[e] University of Bern, Institute of Geological Sciences, Baltzerstrasse 1+3, CH-3012 Bern, Switzerland

ARTICLE INFO

Article history:
Received 28 May 2012
Received in revised form
31 January 2013
Accepted 10 March 2013
Available online 23 March 2013

Keywords:
Lateglacial
Deglaciation history
Exposure dating
^{10}Be and *in situ* ^{14}C

ABSTRACT

We reconstruct the timing of ice flow reconfiguration and deglaciation of the Central Alpine Gotthard Pass, Switzerland, using cosmogenic ^{10}Be and *in situ* ^{14}C surface exposure dating. Combined with mapping of glacial erosional markers, exposure ages of bedrock surfaces reveal progressive glacier downwasting from the maximum LGM ice volume and a gradual reorganization of the paleoflow pattern with a southward migration of the ice divide. Exposure ages of ~16–14 ka (snow corrected) give evidence for continuous early Lateglacial ice cover and indicate that the first deglaciation was contemporaneous with the decay of the large Gschnitz glacier system. In agreement with published ages from other Alpine passes, these data support the concept of large transection glaciers that persisted in the high Alps after the breakdown of the LGM ice masses in the foreland and possibly decayed as late as the onset of the Bølling warming. A younger group of ages around ~12–13 ka records the timing of deglaciation following local glacier readvance during the Egesen stadial. Glacial erosional features and the distribution of exposure ages consistently imply that Egesen glaciers were of comparatively small volume and were following a topographically controlled paleoflow pattern. Dating of a boulder close to the pass elevation gives a minimum age of 11.1 ± 0.4 ka for final deglaciation by the end of the Younger Dryas. *In situ* ^{14}C data are overall in good agreement with the ^{10}Be ages and confirm continuous exposure throughout the Holocene. However, *in situ* ^{14}C demonstrates that partial surface shielding, e.g. by snow, has to be incorporated in the exposure age calculations and the model of deglaciation.

1. Introduction

Reconstructing the extent and dynamics of past glaciers provides valuable information on paleoclimate conditions. The extent of a glacier is determined by the mass balance, which is largely controlled by climate. Variations in the ice volume and glacial expansion therefore give evidence for paleoclimate changes (Oerlemans et al., 1998; Oerlemans, 2001). Being comparatively small ice bodies, Alpine glaciers are particularly sensitive palaeoclimate indicators that respond rapidly to changes in temperature and/or precipitation (Kerschner, 2005).

The onset of the Alpine Lateglacial is defined as the time of massive downwasting of the large valley glaciers built up during the Last Glacial Maximum (LGM; late Würmian) (Penck and Brückner, 1901/1909; Reitner, 2007). Deglaciation of the Alps is thought to have occurred rapidly with retreat of the foreland piedmont glaciers closely followed by the disintegration of the Central Alpine ice cap (Florineth and Schlüchter, 1998; Schlüchter, 2004). Although climate was warming gradually, short climatic fluctuations and cold phases repeatedly interrupted the general trend of ice decay (e.g. Reitner, 2007; Schmidt et al., 2011). These fluctuations are associated with several Lateglacial stadials determined by glacier stillstands and readvances before the beginning of the Holocene warming (Ivy-Ochs et al., 2008 and references therein).

Classically, former extents of Alpine glaciers and related climate changes have been dated by radiocarbon from organic material, mainly retrieved from glacial deposits in the Alpine foreland (e.g.

* Corresponding author. Laboratory of Ion Beam Physics, ETH Zürich, Schafmattstrasse 20, CH-8093 Zürich, Switzerland. Tel.: +41 44 632 47 97; fax: +41 44 632 11 79.
E-mail addresses: hippe@erdw.ethz.ch, hippe@phys.ethz.ch (K. Hippe).

1871-1014/$ – see front matter © 2013 Elsevier B.V. All rights reserved.
http://dx.doi.org/10.1016/j.quageo.2013.03.003

Heuberger, 1966; Patzelt, 1972; Fliri, 1973; Draxler, 1977; Bortenschlager, 1984; Geyh and Schreiner, 1984; Kerschner, 1986; Hajdas et al., 1993; Schlüchter and Röthlisberger, 1995; van Husen, 2004; Keller and Krayss, 2005; Reitner, 2007 and references therein). These data are synchronized with relative chronologies constructed from morpho- and lithostratigraphic observations and fossil and pollen evidence (e.g. Penck and Brückner, 1901/1909; Keller and Krayss, 1987; Ammann et al., 1994; Wohlfarth et al., 1994; van Husen, 2000; Vescovi et al., 2007; Preusser et al., 2011; van Husen and Reitner, 2011). In the last two decades, direct dating of glacial surfaces and moraine deposits by cosmogenic nuclides has provided further valuable information on the chronology of past glacial extents and the timing of glacier retreat (Ivy-Ochs et al., 1996, 2006b, 2007, 2008; Kelly et al., 2006; Hormes et al., 2008; Böhlert et al., 2011; Federici et al., 2012; Reuther et al., 2011). From these data a detailed chronology for the early recession of the LGM ice and the Lateglacial readvances ('stadials') in the Alpine foreland and the inner Alpine valleys was established.

In the high Alps, however, the timing of the breakdown of the LGM ice cap and the extent of Lateglacial local ice is less well constrained. From mapping of glacial trimlines and further glacial erosional features the presence of large, precipitation-controlled ice domes during the LGM has been proposed (Florineth and Schlüchter, 1998, 2000; Kelly et al., 2004a). From the inner Alpine accumulation areas, ice streams expanded into the valleys and glacier transfluences developed at several high Alpine passes (Florineth, 1998; Florineth and Schlüchter, 1998). It is assumed that this ice flow configuration persisted until the piedmont glaciers in the Alpine forelands retreated from their maximum extent (Florineth and Schlüchter, 1998; Kelly et al., 2006). Thus, major downwasting of the inner Alpine ice masses and the termination of glacier transfluence over the high passes were thought to be roughly synchronous to the onset of ice-free conditions in the foreland valleys. However, there is evidence that the high Alps did not deglaciate by that time but that ice persisted locally at high elevations until the beginning of the Bølling/Allerød interstadial (~15–14 ka BP) or even longer (Kelly et al., 2006; Böhlert et al., 2011).

To improve the knowledge about the Lateglacial ice decay in the high Alps and better understand the effect of climate changes on the high Alpine mountain glaciers and ice caps, we performed surface exposure dating of glacially modified bedrock on the Gotthard Pass, central Swiss Alps, using cosmogenic ^{10}Be and *in situ* ^{14}C. Combining ^{10}Be dating with *in situ* ^{14}C analyses takes advantage of the short half-life of ^{14}C (5730 years) which allows to recognize episodes of surface burial as well as constant surface shielding. *In situ* ^{14}C can therefore provide information on the extent of Holocene ice on the Gotthard Pass and can be used to evaluate the necessity of snow shielding corrections for exposure dating in an Alpine environment.

To reconstruct the paleoflow pattern, we combine surface exposure dating with detailed mapping of glacial erosional features in the Gotthard pass area. This yields a detailed chronology of the LGM ice surface lowering and local glacier readvances in conjunction with a progressive reorganization of the glacial ice flow pattern from the LGM until the Holocene.

2. Chronology of the Lateglacial ice decay in the Alps

By ~21 ka the Alpine foreland piedmont glaciers had started to retreat from their maximum position (Schlüchter, 1988, references therein; Schlüchter, 2004; Ivy-Ochs et al., 2004; Preusser, 2004; Keller and Krayss, 2005; Preusser et al., 2011). Deglaciation of the foreland and the inner Alpine valleys by ~19–18 ka marks the beginning of the Alpine Lateglacial (Lister, 1988; Wessels, 1998; van Husen, 2004; Reitner, 2007). According to the work of Reitner (2007) there is no evidence for a climate-driven glacier readvance during the early Lateglacial and therefore the concept of early Lateglacial stadials ('Bühl' and 'Steinach') should be abandoned and replaced by the expression 'phase of early Lateglacial ice decay'. An early Lateglacial phase of warming at ~18.0–17.5 cal ka BP was recorded regionally from southern Alpine macrofossil and pollen data (cf. Vescovi et al., 2007), and by the δ^{18}O in Greenland ice cores (Björk et al., 1998). In the following, a series of prominent moraines were deposited throughout the Lateglacial until the beginning of the Holocene within the Central and Eastern Alps (Maisch, 1981, 1982; Kerschner and Berktold, 1982; Kerschner, 1986).

The first pronounced glacier readvance occurred during the Gschnitz stadial. A maximum age for Gschnitz advances is given by a radiocarbon age of 15.4 ± 0.5 ^{14}C ka BP (19.6–17.6 cal ka BP) from the Eastern Alps (Draxler, 1977). Consistently, exposure ages obtained by ^{10}Be dating of moraine boulders at the type locality in Trins (Gschnitz Valley, Tyol, Austria) as well as from a Gschnitz terminal moraine deposit from the Maritime Alps (Italy) have provided mean ages around 17 ka (Ivy-Ochs et al., 2006a; Federici et al., 2012). Note that these ages and all published ^{10}Be exposure ages discussed below have been renormalized to the 07KNSTD standardization and recalculated using a ^{10}Be spallogenic production rate of 3.93 at g^{-1} y^{-1} (see Section 4.3), without including corrections for erosion or snow, even if these were applied for the original ages. The Gschnitz advance was followed by pronounced glacier downwasting before smaller readvances of the Clavadel/Senders and Daun stadials (Maisch et al., 1999; Ivy-Ochs et al., 2006b; Kerschner, 2009). These readvances were followed by marked ice decay during the Bølling/Allerød interstadial (~14.7–12.9 ka; Björk et al., 1998; Vescovi et al., 2007; Ivy-Ochs et al., 2008) which ended abruptly with the beginning of the Younger Dryas cold period (Ammann et al., 1994; references therein; Rasmussen et al., 2006). Widespread glacier readvance during the Younger Dryas is documented by series of Egesen stadial moraine complexes deposited throughout the Alpine valleys (Kerschner et al., 2000 and references therein). Several surface exposure ages have been obtained from different moraine complexes in Switzerland and Italy. ^{10}Be ages range between ~13.9 and 10.6 ka and are interpreted to give the timing of moraine stabilization during various glacier readvances of the Egesen stadial (Ivy-Ochs et al., 1996, 1999, 2006b; Kelly et al., 2004b, 2006; Federici et al., 2007; Hormes et al., 2008). Several radiocarbon ages of ~11 cal ka BP (summarized and calibrated in Ivy-Ochs et al., 2008) are consistent with ^{10}Be ages and trace the final downwasting of Egesen glaciers. Continued glacier activity into the earliest Holocene is suggested from moraine deposition and rock glacier activity (Fraedrich, 1979; Frauenfelder et al., 2001; Ivy-Ochs et al., 2006b, 2009; references therein; Kerschner and Ivy-Ochs, 2008).

3. Study area

The Gotthard pass is located in Central Switzerland with a pass elevation of 2106 m a.s.l. (Fig. 1). Since the historic past, it has been one of the most important routes traversing the Alps in north-south direction. The Gotthard region comprises crystalline rocks of the Gotthard Massif that forms a part of the crystalline basement of the Swiss Alps. Granitic rocks in the study area are associated with the Fibbia granite gneiss, which is separated by paragneisses from the Gamsboden granite gneiss further north (Labhart, 2009). The Fibbia granite gneiss exhibits a porphyritic texture and syenogranitic composition (Sergeev et al., 1995; Debon and Lemmet, 1999). Plutonic rocks of the Gotthard massif are of Variscan age and were deformed during Alpine orogeny at greenschist to amphibolite facies conditions (Frey et al., 1980; Labhart, 1999).

The pass area shows a typical U-shaped cross section and is characterized by highly polished granitic surfaces and abundant glacial erosional features (Fig. 2). Trimlines at 2640 m a.s.l. on the

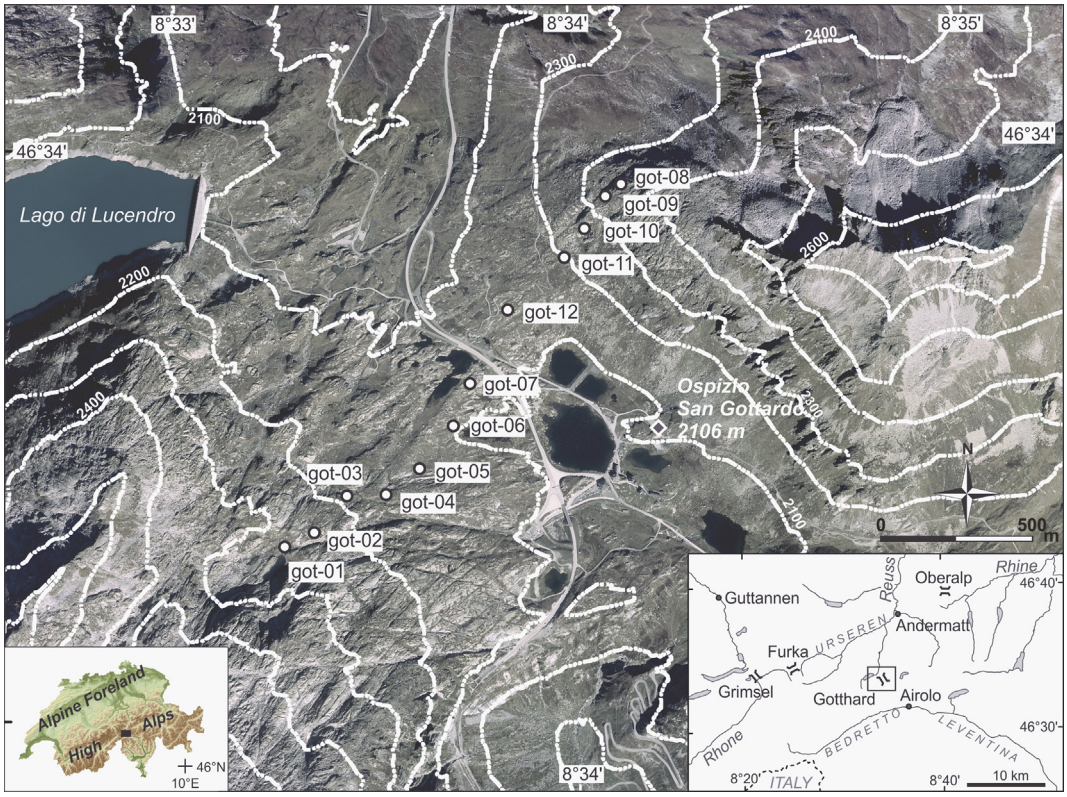

Fig. 1. Modified Landsat image of the Gotthard Pass area showing the sampling locations for surface exposure dating (white circles). The left inset gives the position of the study area within the Swiss Alps. The right inset shows the wider area around Gotthard Pass with its main valleys and passes. Bundesamt für Landestopografie swisstopo.

Pizzo d'Orsino (Fig. 1; Florineth and Schlüchter, 1998) and at ~2500 m a.s.l. at the pass are evidence for the presence of massive ice during the LGM reaching up to 500 m above the pass elevation (Fig. 3). In the northern part of the study area, Lateglacial moraine deposits have been mapped by Renner (1982) and were assigned to the Egesen and Daun stadials (see Discussion). Several Holocene rock glaciers are located in the upper part of the cirque north of Monte Prosa.

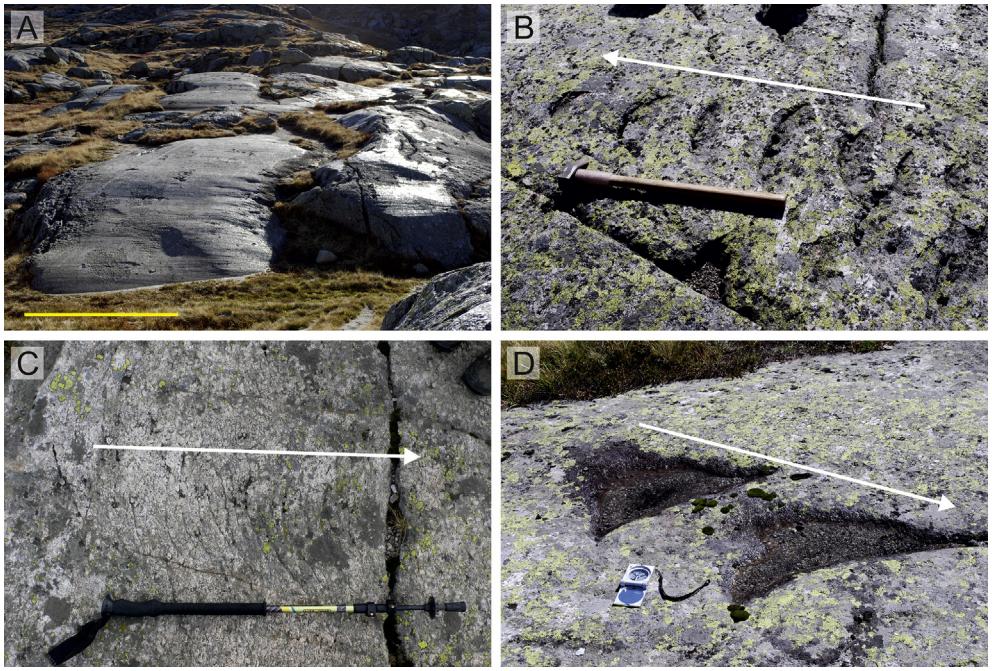

Fig. 2. Glacial erosional features at Gotthard Pass. White arrows indicate the ice flow direction. (A) Glacial striae; yellow scale bar is ~1 m. (B) Row of crescentic gouges. (C) Crescentic fractures. (D) Lunate fractures. (For interpretation of the references to colour in this figure legend, the reader is referred to the web version of this article.)

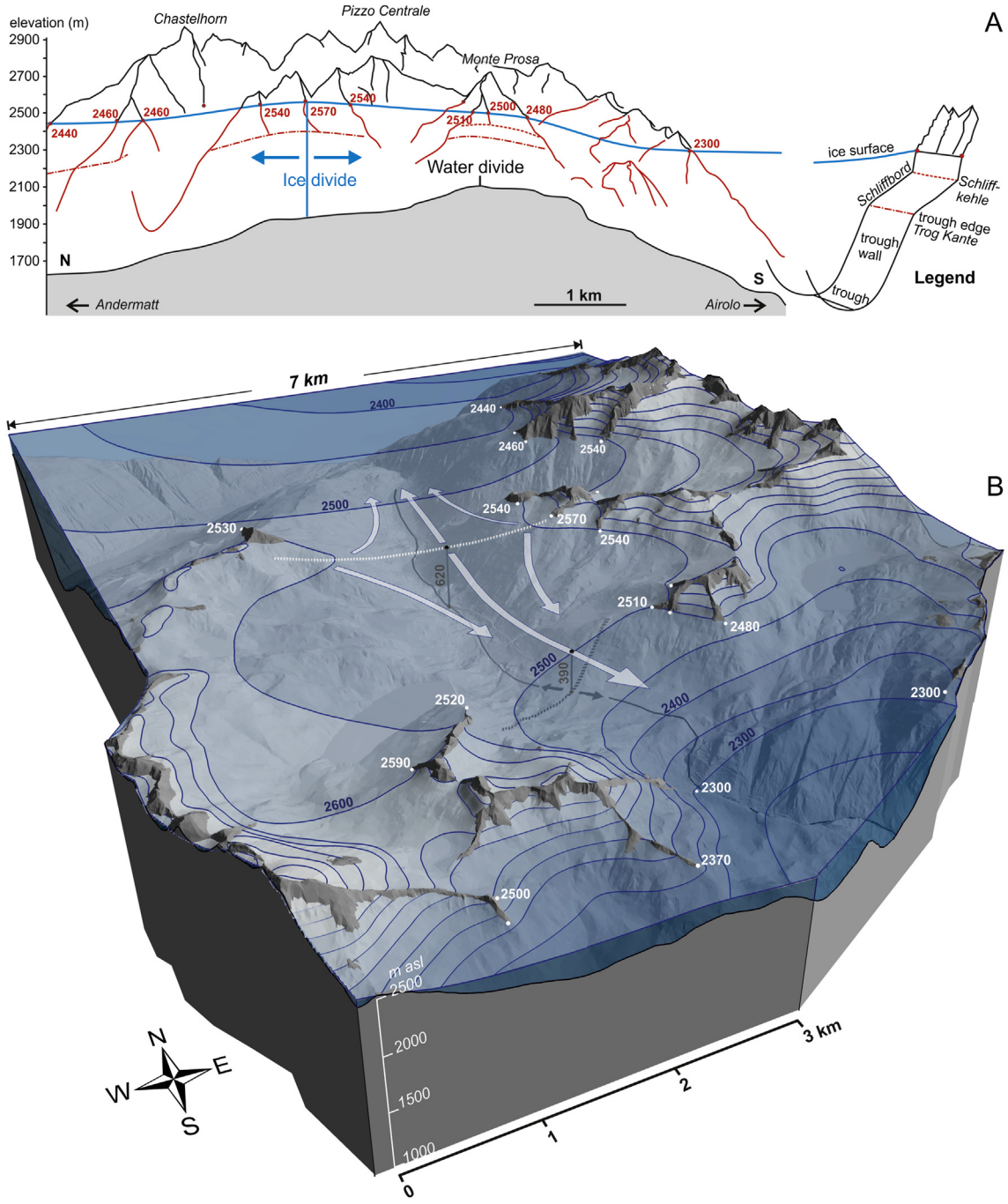

Fig. 3. LGM ice cover of the Gotthard Pass area as reconstructed from trimline mapping. (A) N-S cross-section illustrating the different position of the LGM ice divide in comparison to today's water divide. Red numbers are trimline point elevations. (B) Block diagram showing the ice configuration in the larger pass area. Blue numbers indicate ice surface elevations; white arrows give the direction of ice flow from the ice divide (dashed white line). The grey line represents the thalweg with today's water divide (grey dashed line) and water flow direction (grey arrows) and corresponds to the line of cross-section (A). The vertical black numbers give the thickness of ice at the positions of the LGM ice divide and today's water divide, respectively. Sampling sites for exposure dating closely follow the line of the water divide. (For interpretation of the references to colour in this figure legend, the reader is referred to the web version of this article.)

4. Methods

4.1. Reconstruction of the LGM and Lateglacial ice flow pattern

Two approaches were used to reconstruct the glacier geometry and ice flow pattern in the Gotthard Pass area during and since the LGM: Glacial erosional features were mapped in order to trace the directions of former ice flow, and the LGM ice surface geometry was reconstructed with a GIS-based analysis of glacial trimlines.

In the study area, abundant crescentic fractures and gouges, glacial striae, roches moutonnées and lunate fractures show the direction of past glacier flow (Glasser and Bennett, 2004; Benn and Evans, 2010). During mapping of these features and their interpretation, rows of crescentic gouges were considered most important because their axis of symmetry allows the most accurate reconstruction of the paleoflow direction. Crescentic gouges vary largely in size, depth and state of weathering. At some sites, larger crescentic gouges (up to 1 m wide and several

cm deep) appear more strongly weathered than smaller ones of different direction and were therefore assigned to an older generation that has been overrun by later glacier readvance. Because most glacial striae in the study area are thin and shallow features that often cross-cut comparatively deep crescentic gouges, they are considered to have formed during the last glacier readvance. An example of weathered crescentic gouges cross-cut by younger striae and weakly developed crescentic gouges is given in Fig. 4.

The glacial trimline represents the boundary between an ice-moulded downslope area and a frost-affected upslope zone (Ballantyne, 1990; Florineth, 1998). In high relief mountains as the Alps, this boundary is visible in the morphology of valley-side spurs separating glacial cirques. The maximum extent of ice in main valleys is recorded as a spur truncation showing a more or less sharp transition between the frost-weathered arête zone above the trimline and the gentle ice-moulded ridges and trough shoulders below. In the study area, 19 trimline points were recognized in the field and their detailed position and altitude was extracted from digital elevation models (DEMs) and orthophotomaps. Ice-surface contours with intervals of 25–50 m were drawn for the main valleys with respect to the elevation of the trimline points and considering a concave shape of the ice surface within the accumulation zone. Additionally, ice contour lines directly above the pass were drawn perpendicularly to the direction of the oldest generation of glacial erosional features.

4.2. Sampling and sample preparation

Samples for exposure dating were collected along an altitude transect ranging from 2270 m a.s.l. southwest of Gotthard pass down to pass elevation and up to 2336 m a.s.l. northeast of the pass (Fig. 1; Table 1). Sampling sites follow roughly the line of today's water divide on the pass (Fig. 3). All samples except one (got-05) are from the topmost few centimetres of bedrock surfaces. Sample got-05 was collected from the edge of a $\sim 5 \times 4$ m large and ~ 1–1.5 m high erratic boulder. Glacial polish is most pervasive at bedrock surfaces in the lowermost pass area (around samples got-06, got-07, got-11, got-12). All other surfaces are weakly weathered to slightly pitted with quartz grains standing out a few millimetres. Some surfaces are partially covered by lichens. One glacially polished quartz vein was sampled (got-11).

Fig. 4. Cross-cutting glacial erosional features. Photograph was taken close to sampling site got-08. Two weathered crescentic gouges (next to the compass) indicate southward ice flow and are cross-cut by ENE-WSW-striking glacial striae/polish (direction indicated by the pencil). Two small and weakly developed crescentic gouges (white circle) give the same flow direction as the striae. Another single crescentic gouge (left of the pencil) also points into WSW-direction.

All samples were crushed and sieved to a grain size range of 0.25–1 mm. Quartz mineral separates were prepared and purified by leaching in HCl and weak HF following the methods described in Kohl and Nishiizumi (1992) and Ivy-Ochs (1996). Samples were spiked with 0.3 g ^{9}Be and dissolved in concentrated HF. ^{10}Be was separated from $\sim$30 to 70 g quartz using ion exchange column chemistry according to Ivy-Ochs (1996). The ^{10}Be/^{9}Be ratio was measured at the ETH Zürich 6 MV Tandem accelerator mass spectrometry (AMS) facility (Synal et al., 1997; Kubik and Christl, 2010). Subtracted ^{10}Be/^{9}Be blank ratios were on the order of 3×10^{-15}. *In situ* ^{14}C was extracted from $\sim$5 g quartz by heating at 1550–1600 °C as described in Hippe et al. (2009, 2013). Extraction was initially performed in two subsequent, high-T heating steps. For both steps, concentrations were measured separately and then added to a total ^{14}C concentration for the sample (Table 2). Later, ^{14}C was extracted in one single heating step (cf. Hippe et al., 2013). Subtracted long-term processing blanks were $(2.81 \pm 1.02) \times 10^{4}$ ^{14}C atoms ($\pm$1 st dev, $n = 11$) for the first and $(1.48 \pm 0.66) \times 10^{4}$ ^{14}C ($\pm$1 st dev, $n = 10$) for the second extraction step, respectively, and $(4.55 \pm 2.19) \times 10^{4}$ ^{14}C ($\pm$1 st dev, $n = 9$) for the modified extraction method. Samples were measured at ETH Zürich with the MICADAS AMS system using a gas ion source (Ruff et al., 2007; Synal et al., 2007; Wacker et al., 2010).

4.3. Exposure age calculation

To calculate ^{10}Be exposure ages a sea level-high latitude (SLHL) spallogenic production rate of 3.93 ± 0.19 at g^{-1} a^{-1} was applied, based on the Northeast North America calibration data of the CRONUS-Earth online calculator (Balco et al., 2008). This value was chosen in view of a number of recently published production rate data that suggest a ^{10}Be production rate for spallation in the northern hemisphere on the order of 3.7–4.3 at g^{-1} a^{-1} (Lal, 1991/Stone, 2000 scaling; Balco et al., 2009; Lifton et al., 2009; Fenton et al., 2011; Goehring et al., 2011; Briner et al., 2012). *In situ* ^{14}C exposure ages were calculated with a SLHL spallogenic production rate of 12.29 ± 0.99 at g^{-1} a^{-1} (Lifton, pers. comm.), which is based on a re-evaluation of the published *in situ* ^{14}C calibration data (Lifton et al., 2001; Miller et al., 2006; Dugan, 2008) using the total muonic production rates as given in Heisinger et al. (2002b). The contribution due to muon production was calculated independently using the freely accessible MATLAB code of the CRONUS-Earth online calculator (Balco et al., 2008), which implements the method of Heisinger et al. (2002a,b) for altitude and depth scaling. Parameters were adjusted to allow muon scaling for ^{10}Be and *in situ* ^{14}C using the revised muon interaction cross sections for ^{10}Be as specified in Balco (2009) and cross sections for ^{14}C as published in Heisinger et al. (2002a,b).

Spallogenic production rates were scaled to altitude and latitude according to the scaling scheme of Lal (1991)/Stone (2000). No correction was done for geomagnetic field intensity variations because their effect on the production rates is assumed negligible at latitudes >40° (Masarik et al., 2001). Corrections for sample thickness was applied on spallogenic production only assuming an exponential decrease of production with depth and using an effective attenuation length Λ_{sp} of 160 g cm^{-2} and a rock density of 2.65 g cm^{-3}. The attenuation of muons within the uppermost few centimetres below the surface is small and can be reasonably ignored. Correction factors for topographic shielding and sample geometry were derived according to Dunne et al. (1999). An additional correction for snow cover was performed for some samples and will be discussed in detail in Section 5.3. Correction factors for snow shielding were calculated using equation (after Gosse and Phillips, 2001):

Table 1
Sample information and the measured ^{10}Be concentrations.

Sample ID	Latitude (°N)	Longitude (°E)	Elevation (m a.s.l.)	Sample thickness (cm)	Topographic shielding factor[a]	^{10}Be concentrations (10^4 at g^{-1})[b]
got-01	46.5539	8.5539	2270	3	0.821	27.35 ± 1.35
got-02	46.5541	8.5546	2252	1	0.986	26.13 ± 1.14
got-03	46.5553	8.5556	2195	4	0.986	27.28 ± 1.30
got-04	46.5557	8.5579	2166	4	0.987	25.55 ± 1.20
got-05	46.5564	8.5587	2140	4	0.993	23.93 ± 0.96
got-06	46.5572	8.5601	2120	4	0.993	30.79 ± 1.02
got-07	46.5582	8.5611	2116	3	0.992	24.50 ± 1.09
got-08	46.5641	8.5670	2336	2	0.980	33.23 ± 1.14
got-09	46.5637	8.5664	2324	4	0.992	31.64 ± 1.37
got-10	46.5628	8.5658	2250	2	0.936	29.76 ± 1.26
got-11	46.5619	8.5653	2197	2	0.972	23.75 ± 1.11
got-12	46.5605	8.5628	2135	3	0.987	24.23 ± 1.08

[a] Correction factor calculated according to Dunne et al. (1999) including shielding due to the dip of the sampled surface and the shielding by the surrounding topography.
[b] Errors are at the 1σ level and include the AMS analytical uncertainties and the error of the subtracted blank. Measured ratios were normalized to the S2007N standard (calibrated to 07KNSTD) using a half-life of 1.387 ± 0.012 (Chmeleff et al., 2010; Korschinek et al., 2010).

$$S_{\mathrm{snow}} = \frac{1}{12}\sum_{\mathrm{i}}^{12} \mathrm{e}^{-\left(z_{\mathrm{snow,i}}\cdot\rho_{\mathrm{snow}}/\Lambda_{\mathrm{sp}}\right)}, \quad (1)$$

where $z_{\mathrm{snow,i}}$ is the monthly average snow depth (cm) and ρ_{snow} is the snow density, for which we used an average value of 0.3 g cm^{-3}. Any snow shielding corrections were applied on the spallogenic production only because of the comparatively small attenuation effect of snow on the muonic production (cf. Schildgen et al., 2005). Because of the abundant well-preserved glacial erosional features in the study area, surface erosion since exposure was considered to be negligible.

5. Results

Sample information and measured concentrations are given in Table 1 for ^{10}Be and Table 2 for *in situ* ^{14}C. Exposure ages are summarized in Table 3 and Fig. 5. Given errors are at the 1σ level including the AMS counting error and the error associated with the subtracted blank. For *in situ* ^{14}C, an additional uncertainty of 4% was included to account for analytical variability in the *in situ* ^{14}C extraction procedure (Hippe et al., 2013).

Exposure ages obtained from ^{10}Be range from 10.7 ± 0.5 ka to 14.5 ± 0.5 ka. Consistently, ages of eight samples analysed for *in situ* ^{14}C vary from 9.2 ± 0.4 ka to 14.6 ± 0.6 ka and cover about the same age range as obtained from ^{10}Be. These ages represent minimum estimates for deglaciation of the Gotthard Pass area suggesting that at latest by the beginning of the Holocene the Gotthard Pass area was completely ice-free. The overall agreement between ^{10}Be and *in situ* ^{14}C ages is illustrated in the ^{10}Be/^{14}C vs. ^{14}C diagram (Fig. 6), in which all data points cluster around the line of constant exposure suggesting a simple exposure history throughout the Holocene. For individual samples, differences between ^{10}Be and *in situ* ^{14}C ages are between ~1 and 3 ka but show no clear trend, i.e. some ^{14}C ages are younger, some are slightly older than the corresponding ^{10}Be ages. Including production rate uncertainties (~5 and 8% for ^{10}Be and ^{14}C, respectively), ages from both nuclides are equal for each sample (Fig. 6A). However, we suppose that the small differences between ^{10}Be and *in situ* ^{14}C results can provide important information about snow (or sediment) cover and should be discussed

Table 2
In situ ^{14}C data[a]. All errors are at the 1σ-level.

Sample ID (AMS ID)	Sample mass (g)	CO_2 yield (μg)[b]	Fraction modern $F^{14}C$[c]	$\delta^{13}C$ (‰)	$^{14}C/^{12}C_{abs}$ (10^{-12})[d]	^{14}C (10^5 at g^{-1})[e]
got-01a (41519.01)	5.23	4.7 (–)	7.164 ± 0.067	−11.43	8.682 ± 0.081	3.82 ± 0.06
got-01b (41519.02)	5.23	0.7 (8.2)	0.638 ± 0.012	−52.90	0.710 ± 0.013	0.57 ± 0.02
Total						4.39 ± 0.06
got-04 (42438.2.1)	5.21	14.7 (–)	2.688 ± 0.009	3.4	3.359 ± 0.029	4.63 ± 0.05
got-05a (41518.01)	4.85	5.1 (–)	6.917 ± 0.058	−11.95	8.383 ± 0.071	4.36 ± 0.06
got-05b (41518.02)	4.85	0.9 (7.4)	0.433 ± 0.010	−49.73	0.486 ± 0.011	0.38 ± 0.02
Total						4.74 ± 0.07
got-06 (45656.1.1)	5.37	33.9 (–)	1.227 ± 0.013	−11.09	1.489 ± 0.016	4.61 ± 0.06
got-07a (42439.01)	4.92	7.9 (–)	4.032 ± 0.028	−15.20	4.853 ± 0.034	3.72 ± 0.04
got-07b (42439.02)	4.92	1.1 (7.3)	0.749 ± 0.012	−44.51	0.849 ± 0.013	0.67 ± 0.02
Total						4.39 ± 0.05
got-08 (45653.1.1)	5.04	9.1 (–)	5.116 ± 0.044	−15.35	6.156 ± 0.052	5.47 ± 0.06
got-10 (45655.1.1)	5.12	7.1 (–)	6.592 ± 0.062	−23.05	7.809 ± 0.074	5.33 ± 0.07
got-11 (45654.1.1)	5.03	4.7 (–)	7.901 ± 0.108	−24.85	9.325 ± 0.128	4.30 ± 0.08

[a] For samples got-01, got-05, and got-07 the results of both extraction steps and the total concentration are given. Samples got-04, got-06, got-08, got-10, got-11 were extracted in one single heating step.
[b] Numbers in brackets give amount of 'dead' CO_2 gas added. Uncertainty deriving from the CO_2 pressure reading is 0.07 μg.
[c] Normalized to $\delta^{13}C$ of −25‰ VPDB and AD 1950.
[d] Calculated after Eq. (1) in Hippe et al. (2013).
[e] Calculated after Eq. (2) in Hippe et al. (2013). Blank corrected and corrected for the addition of 'dead' CO_2 gas with a mean ^{14}C concentration of 315 ± 118 at μg^{-1} CO_2 (1σ, n = 12).

Table 3
Calculated exposure ages for the Gotthard samples. All errors are at the 1σ-level and include analytical uncertainties only (including blank error). For *in situ* ^{14}C ages 4% uncertainty was added to account for analytical reproducibility.

Sample ID	^{10}Be exposure age (years)	^{10}Be snow corrected nexposure age (years)[a]	^{14}C exposure age (years)	^{14}C snow corrected exposure age (years)[a]
got-01	13920 ± 690	15200 ± 750	12050 ± 510	14610 ± 620
got-02	11100 ± 480	12080 ± 530	–	–
got-03	12310 ± 580	13450 ± 640	–	–
got-04	11750 ± 550	12840 ± 600	11100 ± 460	13280 ± 550
got-05[b]	11140 ± 450		12000 ± 510	
got-06	14540 ± 480	15880 ± 530	11570 ± 480	13940 ± 580
got-07	11510 ± 510	12570 ± 560	10390 ± 430	12290 ± 510
got-08	13470 ± 460	14720 ± 510	12290 ± 510	15020 ± 630
got-09	12990 ± 560	14190 ± 620	–	–
got-10	13390 ± 570		14640 ± 620	
got-11	10670 ± 500	11660 ± 540	9180 ± 410	10690 ± 470
got-12	11290 ± 500	12330 ± 550	–	–

[a] Corrected for 100 cm of snow during 6 month per year ($\rho_{snow} = 0.3$ g cm^{-3}) using Eq. (1). Samples got-05 and got-10 were not corrected for snow shielding according to the results shown in Fig. 6B.
[b] Boulder.

independently of the intrinsic uncertainties for the production rates. In the following, we will discuss the observed spread in exposure ages and evaluate the information on snow shielding gained from the combined ^{10}Be-^{14}C data.

6. Discussion

6.1. Overall trends in the exposure ages

Exposure ages from ^{10}Be and *in situ* ^{14}C show a trend towards older ages at higher elevations along the north-eastern pass side with oldest ages recorded from locations above 2250 m (got-08, got-09, got-10; Fig. 5). Nuclide inheritance has been proposed as one possible interpretation for such a pattern (Fabel et al., 2004). This means that the LGM ice would not have eroded the bedrock deeply enough at these sites to completely remove cosmogenic nuclides that have accumulated during pre-LGM surface exposure. Different studies have shown that the spatial pattern and rate of glacial erosion can vary significantly within a landscape depending, e.g., on the thermal regime of the ice (Fabel et al., 2002; Stroeven et al., 2002), the position within the valley (Fabel et al., 2004), or the bedrock type and fracturing (Dühnforth et al., 2010). Erosion rates beneath modern temperate glaciers are estimated to be at least 1 mm y^{-1} for mid-latitude regions (e.g. Small, 1987; Nesje et al., 1992; Hallet et al., 1996; references therein; Riihimaki et al., 2005). This would be sufficient to remove several meters of bedrock during the LGM and erase the pre-glacial nuclide inventory. From trimline elevations in the Gotthard Pass area we estimate that even the highest sampling sites were at least 100 m below the LGM ice surface. Furthermore, the fact that the oldest exposure age was obtained from a sampling site close to pass elevations (got-06) strongly argues against nuclide inheritance. This site in the central pass area was covered by about 400 m of ice (Fig. 3) and is situated in between two sampling sites that yielded about 3 ka younger ages (got-04, got-07). Field evidence does not suggest markedly variable glacial erosion for these sampling sites or generally within the entire study area. Also, there is no obvious trend in the age distribution on the south-western pass side. We therefore propose that the observed spread in exposure ages does not result from nuclide inheritance but reflects more than one episode of ice surface lowering and deglaciation in the Gotthard Pass area. This will be presented in detail in Section 7.

6.2. Combined ^{10}Be-^{14}C data

In mountainous regions, the recognition of surface shielding by snow and an appropriate snow correction can be crucial for the calculation of accurate surface exposure ages (cf. Schildgen et al.,

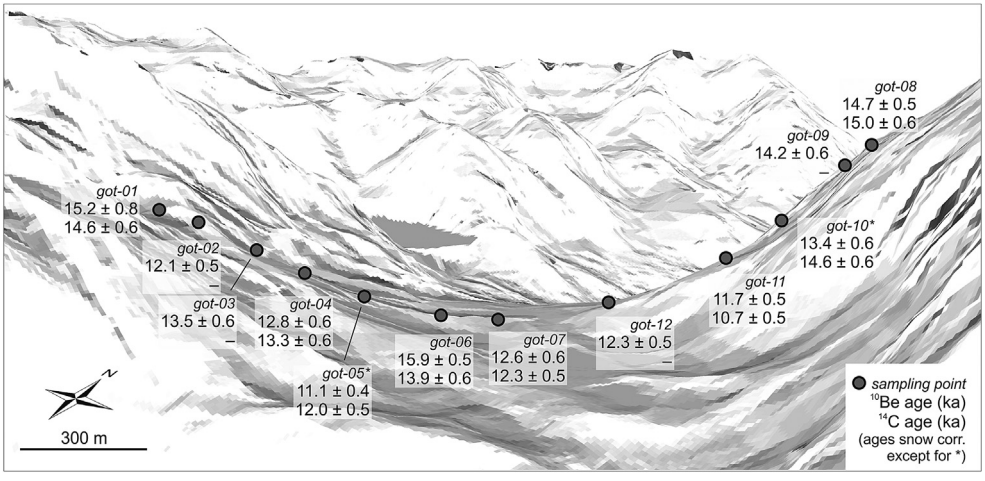

Fig. 5. Relief map with the sampling sites and surface exposure ages (in ka) as obtained from ^{10}Be and *situ* ^{14}C analysis. Ages are corrected for 1 m of snow during 6 month per year (except for got-05 and got-10). Bundesamt für Landestopografie swisstopo.

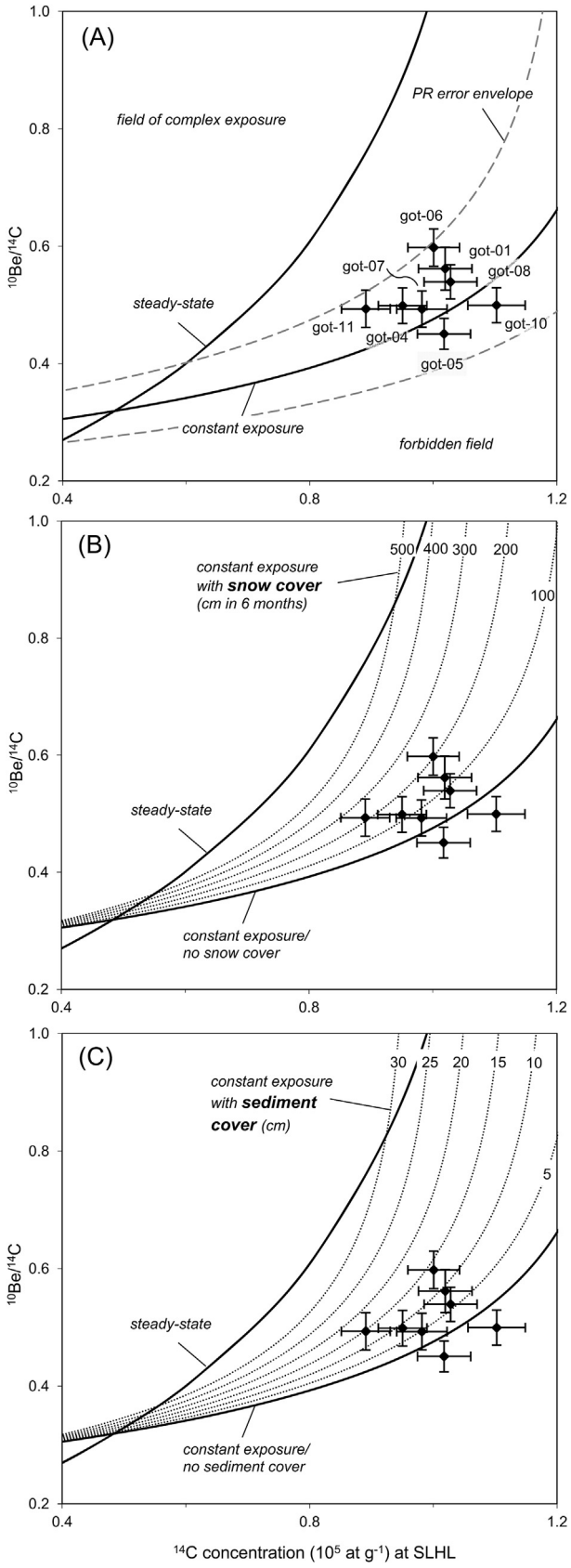

Fig. 6. Results for samples analysed for ^{10}Be and *in situ* ^{14}C plotted in ^{10}Be/^{14}C vs. ^{14}C diagrams. Error bars represent 1σ analytical uncertainty including errors on the subtracted blank and 4% uncertainty for *in situ* ^{14}C to account for reproducibility. All samples plot close to the line of simple exposure and show a general agreement between ^{10}Be and *in situ* ^{14}C data. (A) Including the current production rate uncertainties, marked with grey dashed lines, ^{10}Be and *in situ* ^{14}C exposure ages would be identical within 1σ. (B) Considering only the analytical uncertainties, *in situ* ^{14}C exposure ages that are slightly younger than the ^{10}Be ages, i.e. samples plotting left of the constant exposure line, could be explained by Holocene snow cover. Dotted lines are lines of constant exposure that include permanent shielding due to snow cover (Eq. (1), $\rho = 0.3$ g cm^{-3}). (C) Alternatively to (B), slightly younger *in situ* ^{14}C ages can also be caused by shielding due to a thin sediment (till) layer ($\rho = 2.0$ g cm^{-3}).

2005; Böhlert et al., 2011; Fenton et al., 2011). As snow cover reduces the cosmogenic nuclide production rate, ignoring the presence of snow can cause a systematic underestimation of exposure ages. However, a correction for snow shielding usually involves large uncertainties because no direct information on past snow depths is available and any assumptions have to rely on historic climate data (e.g., Gosse and Phillips, 2001). Here, the combination of ^{10}Be with *in situ* ^{14}C provides the opportunity to check on the necessity and extent of a shielding correction for exposure dating of the Gotthard Pass. Because of its short half-life, the *in situ* ^{14}C concentration approaches secular equilibrium much faster compared to the long-lived ^{10}Be. Also the contribution by muons to the total production rate is significantly higher for *in situ* ^{14}C. Therefore, snow cover and the correction of exposure ages for snow shielding has a much stronger effect on calculated *in situ* ^{14}C ages compared to ^{10}Be.

As shown in the two–isotope diagram (Fig. 6), data points for 6 of 8 samples plot above the line of constant exposure/no erosion (no shielding by snow or sediment). For those samples that yielded slightly lower *in situ* ^{14}C than ^{10}Be ages (got-01, got-04, got-06, got-07, got-08, got-11), partial surface shielding is indicated. Assuming constant snow depths throughout the Holocene, measured concentrations of both nuclides can be brought into agreement for a variable amount of snow cover of ~80–200 cm during 6 months per year (Fig. 6B). Two samples (got-06, got-11) agree with the modern snow depth of ~180 cm during 6 months per year as deduced from the mean Nov–April snow depths recorded from 1983 to 2002 at climate stations nearby (data from the Institute for Snow and Avalanche Research and MeteoSwiss; Auer, 2003). The other four samples indicate only about half to two-thirds of the amount of snow throughout the Holocene, which is consistent with the suggested warmer climate during the middle Holocene (Hormes et al., 2001; Davis et al., 2003; references therein, Joerin et al., 2006). Finally, data points for two other samples (got-05, got-10) do not plot above line of constant exposure/no erosion implying that no further shielding correction is needed for these sites. With sample got-05 collected from the edge of a boulder and sample got-10 from a 30° dipping surface, these results are very reasonable.

In addition to snow cover, surface shielding by glacial sediment (till) could be considered. Although no sediment cover exists at the sampling sites at present, it cannot be excluded that patches of till covered the now exposed bedrock during an unknown time interval right after deglaciation. Shielding by sediment could explain some differences observed for adjacent sites on the pass (e.g., got-06 and got-07). It may also be possible that the well-preserved glacial polish around the low-elevation sites results from surfaces being protected by an initial sediment layer now eroded. Assuming constant shielding by sediment only (no snow), about ~10–20 cm thick till is required to explain the measured differences in the ^{10}Be and *in situ* ^{14}C concentrations (Fig. 6C). However, we assume snow to be the main shielding element and till to be of minor influence, if any.

Furthermore, the fact that data points for samples got-05, and got-10 plot below the line of constant exposure/no erosion could imply that the *in situ* ^{14}C spallogenic production rate might be

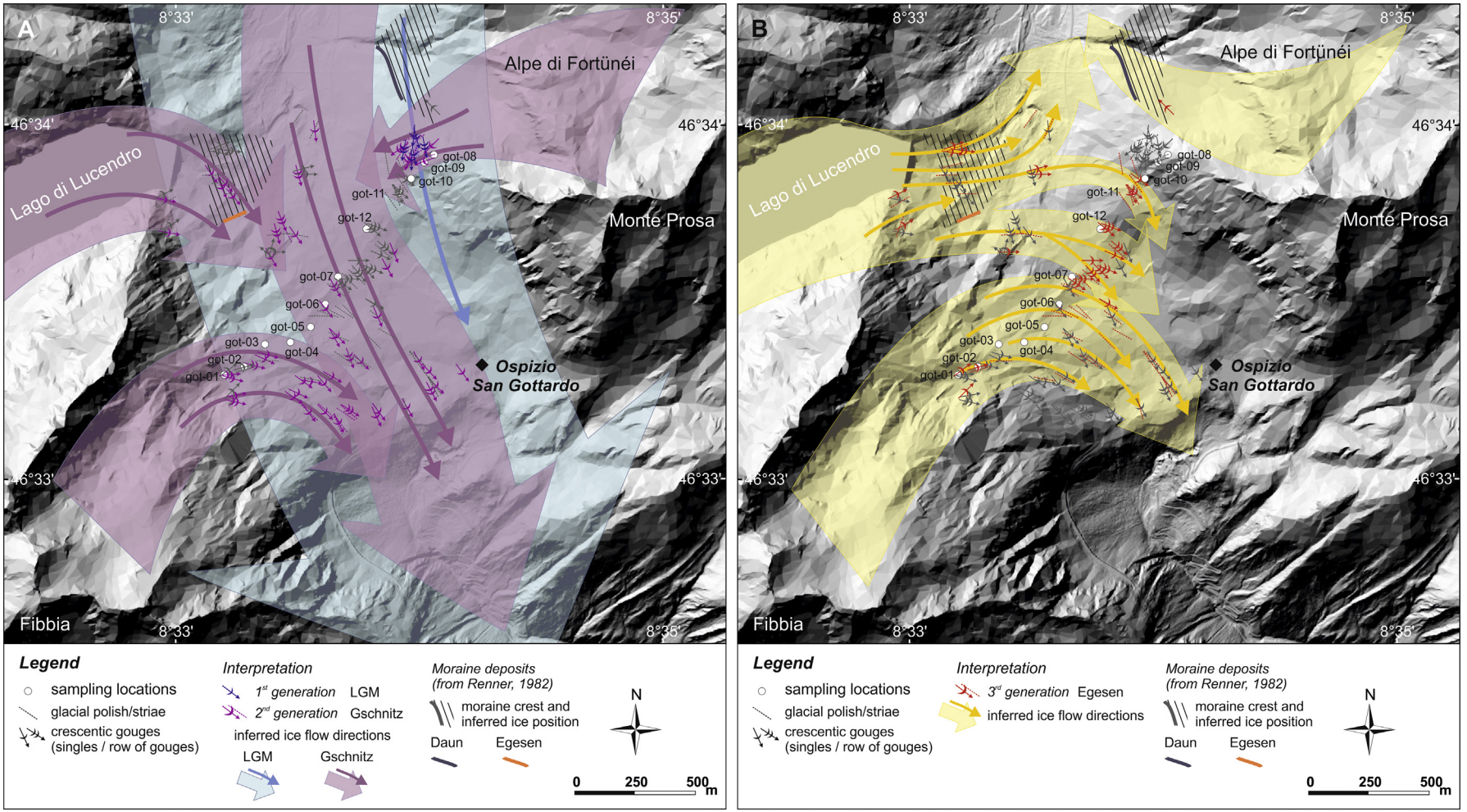

Fig. 7. Reconstructions of generalized ice flow pattern for the LGM and the Gschnitz stadial of the Oldest Dryas (A), and for the Egesen stadial of the Younger Dryas cold period (B), based on glacial erosional markers.

slightly underestimated. A production rate determined from the combined ^{10}Be and ^{14}C data of samples got-05, and got-10 would be around 12.8 at g^{-1} y^{-1}, which is well within the uncertainty of the current spallogenic production rate of 12.29 ± 0.99 at g^{-1} y^{-1}. However, a higher production rate would also implicate increased surface shielding corrections for the other samples.

Altogether, combining ^{10}Be with *in situ* ^{14}C analyses may yield more accurate surface exposure ages as it provides a tool to identify surface shielding and to estimate the amount of snow correction. We have corrected all exposure ages (except got-05 and got-10) for snow cover using a minimum snow depth of 100 cm in 6 months as suggested from our combined ^{10}Be-^{14}C data (Fig. 6B). Overall, these corrections increase the ^{10}Be ages by ~1 ka and *in situ* ^{14}C ages by ~2–3 ka (Table 3).

7. Surface exposure ages in the context of paleoflow reconstruction

Snow corrected exposure ages from the Gotthard Pass suggest a successive deglaciation of the pass area during the Lateglacial. Deglaciation started at ~16–15 ka and the pass became completely ice-free at the beginning of the Holocene by ~11 ka. Using field observations of glacial erosional features, exposure age data will be linked in the following to changes of ice volume and paleoflow directions throughout the period of Lateglacial ice decay. Results from the mapping of erosional markers are presented in Fig. 7A and B, which summarize our interpretation of these markers and illustrate the conclusions on the glacial flow pattern. At most sites on the pass two generations of erosional features occur in a cross-cutting pattern. We interpret these to correspond altogether to three generations of erosional markers and, thus, to document three different paleoflow patterns.

7.1. LGM

Landscape topography and strongly abraded bedrock surfaces on the Gotthard Pass record an intensive glacial imprint by highly erosive ice masses. Within the central pass area up to 1 m large, few cm deep and often weathered crescentic gouges are superimposed on the erosional bedforms. These features are consistent with the proposed LGM flow pattern into SSE direction (Fig. 3; cf. Florineth and Schlüchter, 1998) but could also have formed during later glacial stages. The only site where the first generation of erosional markers can be clearly identified is on the ridge south of the Alpe di Fortünéi, where SSE to SSW-directed crescentic gouges are cross-cut by SW to WSW-pointing crescentic gouges and parallel running glacial striae (Fig. 4 and Fig. 7A). The older generation of erosional features implies a roughly S-directed ice flow, which does not follow local topography and agrees with the LGM flow pattern. As suggested by our reconstruction of the LGM glacial cover illustrated in Fig. 3, the LGM ice divide was about 2 km north of today's water divide on the Gotthard Pass. Glacier transfluence over the pass was forced by the dynamics of the enormous ice masses originating from the cirques north of the Monte Prosa and at the Lago di Lucendro that served as main accumulation areas. North of the ice divide, glacier transfluences existed at the Oberalp and Furka passes into the direction of the Urseren valley (Fig. 1). From there, the ice was draining northwards into the Reuss glacier. Although a lowering of the LGM ice surface at Gotthard Pass is suggested from field evidence (see below), our exposure ages do not record ice-free conditions during the early Lateglacial.

7.2. Oldest Dryas

Small and shallow crescentic gouges that are less weathered, fine glacial striae and glacial polish represent a younger generation of erosional features that show variable directions of ice flow deviating from the main LGM flow direction. This second generation of erosional markers (SW to WSW-directed) imply a change in the ice flow configuration, most likely after a significant decrease of the ice elevation, and suggests the presence of a local glacier at the Monte Prosa. However, because the glacial ice from the Monte Prosa cirque is continuously flowing opposite to topography, the persistence of a large ice mass on the pass is required to force local glaciers into the predominant southward direction. The termination of the ice flow over the ridge south of the Alpe di Fortünéi represents the timing of severe glacier downwasting and is constrained by the exposure ages of got-08 and got-09 that give a mean age of 14.5 ± 0.8 ka (Fig. 7). Based on the large volume of ice implied by the pattern of the glacial erosional features these exposure ages are interpreted to portray the downwasting of Gschnitz stadial glaciers. These are envisioned as a large system of transection glaciers with a pattern similar to the LGM but limited to the high elevation inner Alpine valleys. Crescentic gouges east of the Lago di Lucendro (Fig. 7A) suggest that local ice coming out of the lake depression was forced to flow towards SE opposite to topography. Thus, erosional markers are considered to have formed at the same time as the ones assigned to the second generation on the ridge south of the Alpe di Fortünéi. Erosional features in the SW of the pass agree with this flow pattern. Approaching pass elevation, the ice flow direction recorded by the erosional markers gradually changes from the initial E-ENE direction into a SSE-ward flow. However, as this pattern follows the general topography, these markers must not necessarily have formed contemporaneously with the second generation of erosional features further north. Nevertheless, abundant deep (few cm) crescentic gouges point to a quite large volume of ice that caused strong glacial erosion (cf. Glasser and Bennett, 2004). Within this configuration the ice divide was still situated north of Gotthard Pass.

An exposure age of 15.2 ± 0.8 ka obtained from the highest sampling site at the south-eastern pass side (got-01) suggests an overall synchronous deglaciation of the pass area. Altogether, these ages propose that glacier transfluence persisted in the Gotthard Pass area throughout the Oldest Dryas and that the large system of local transection glaciers decayed even as late as the onset of the Bølling/Allerød interstadial.

7.3. Younger Dryas

An apparent third generation of erosional features is well defined east of the Lago di Lucendro by ~E-W-striking glacial polish cross-cutting the second generation of crescentic gouges (SE-directed). These features clearly show a major reorganization of the paleoflow pattern into a nearly completely topographically controlled system and a shift of the ice divide towards the south close to today's water divide. During this phase of glacier readvance local ice from the Lago di Lucendro moved down-valley towards the north as well as eastwards across the pass. Consistently, a single but not very well developed crescentic gouge at the Alpe di Fortünéi is indicating northwards glacial flow out of the cirque following local topography. A left lateral moraine within the Alpe di Fortünéi, which may have formed during this readvance, was mapped by Renner (1982) and attributed to the Daun stadial (Fig. 7B).

Rows of comparatively small and shallow (few mm) crescentic gouges around sampling site got-12 suggest a much smaller glacier system with little erosional potential but also indicate that ice from the Lago di Lucendro valley spread over a large part of the northern

pass area. In agreement with field observations, samples got-11 and got-12, that were located within the lower pass area below 2200 m a.s.l., yielded younger ^{10}Be ages of 11.7 ± 0.5 ka and 12.3 ± 0.5 ka, respectively. These suggest an attribution of the third generation of erosional markers with the Younger Dryas cold phase and to a readvance of Egesen stadial glaciers. This supports the interpretation of Renner (1982) that the right lateral moraine east of the Lago di Lucendro (Fig. 7B) was deposited during the Egesen stadial. Consistently, readvance of local ice at the southwestern pass side was dated to 12.1 ± 0.5 ka to 12.8 ± 0.6 ka (got-02, got-04, got-07). Finally, a minimum age of 11.1 ± 0.4 ka for the final deglaciation of the Gotthard Pass is given from the boulder (got-05) and is consistent with deposition during Egesen advance and ice-free conditions by the end of the Younger Dryas. This age is also in good agreement with radiocarbon dates from the Central Alps indicating ice-free conditions at elevations of ~2150 m by ~11.2–12.6 cal ka BP (Renner, 1982).

Glacial striae (E-W to SE-NW-striking) that cross-cut older crescentic gouges in the central pass area clearly demonstrate that local ice was expanding from the cirque north of the Piz Lucendro (Fig. 7B) at some time after the breakdown of the large Gschnitz glacier system. This pattern of striae right at the pass documents the dominance of local glaciers and indicates the absence of a large, south-flowing glacier in that area. Although all sampling sites in the southwestern study area are located below the cirque basin north of the Piz Lucendro, not all samples yielded Egesen stadial ages. We suggest that the spread in ages documented on this side of the pass results from a first exposure of all sites starting at ~16 ka and only a partial coverage by readvancing Egesen glaciers. The Younger Dryas was a ~1.1–1.3 ka long, climatically unstable period (Alley, 2000). In some regions of the Alps up to seven Egesen moraines with intervening periods of ice recession have been identified (Maisch, 1982, 1987; Kerschner et al., 2000 and references therein). Because of the flat topography of the pass area, during each advance the glacier may have followed a slightly different path leading to some areas being covered and others not.

8. Conclusions

In this study ^{10}Be and *in situ* ^{14}C exposure dating were combined with mapping of glacial erosional features to elucidate the pattern of deglaciation of the Gotthard Pass after the LGM. Erosional markers suggest a progressive glacier downwasting from the maximum LGM ice volume and a gradual re-organization of the ice flow pattern with a southward migration of the ice divide. Glacial trimlines record the enormous ice volume that accumulated during the LGM and that forced glaciers into an exclusively SSE-directed flow. With downwasting of the LGM ice, the glacial regime changed into a system of large interconnected dendritic glaciers that seems to have continuously followed the general LGM paleoflow direction. This phase of early ice decay (cf. Reitner, 2007) can be clearly identified from field evidence but is not recorded by the exposure ages. The oldest obtained ^{10}Be exposure ages from samples above 2250 m a.s.l. indicate first local deglaciation between 15.2 ± 0.8 ka and 14.2 ± 0.6 ka. These ages can be attributed to the decay of the large Gschnitz glacier system by the end of the Oldest Dryas. From these data it is suggested that although the ice volume was decreasing by the end of the LGM, large transection glaciers persisted in the Gotthard region throughout the Oldest Dryas allowing glacier transfluence over the pass. These results are in good agreement with bedrock exposure ages reported from the high Alpine Grimsel and Albula passes (Kelly et al., 2006; Böhlert et al., 2011) implying that the scenario of rapid deglaciation by the end of the LGM, as recorded for the Alpine foreland, does not reflect the conditions in the high Alps. Glaciers remained large in high elevation areas for several thousand years after downwasting of the foreland piedmont glaciers and possibly decayed as late as the onset of the Bølling warming.

After drastic downwasting of the ice volume during the Bølling/Allerød interstadial, local glaciers readvanced during the Younger Dryas cold phase forming an entirely topographically controlled ice flow pattern with ice flowing out of the cirques. ^{10}Be exposure ages of ~12–13 ka give the timing of Egesen glacier readvance (cf. Ivy-Ochs et al., 2009). Egesen glaciers expanding from the higher elevated accumulation areas covered most of the pass area. However, glacial erosion was negligible. From the recorded spread in ^{10}Be exposure ages we assume that the Egesen readvance was preceded by an episode of ice-free conditions during part or all of the Bølling/Allerød interstadial. Thus, some sites have been pre-exposed during that time. Egesen glaciers may not have equally covered the entire area due to local variations in tongue geometry. The timing of final deglaciation by the end of the Younger Dryas is constrained by the ^{10}Be minimum exposure age of 11.1 ± 0.4 ka from the only analysed boulder (got-05) that was deposited during the last glacier readvance.

From the combination of ^{10}Be and *in situ* ^{14}C data, we were able to evaluate the necessity of a snow shielding correction. Detailed constraints on the amount of such a correction were gained for each sampling site. The overall consistency between the *in situ* ^{14}C and the ^{10}Be data excludes the presence of significant glacial ice (including non-erosive ice patches) for any time on Gotthard Pass during the Holocene and points to a continuous exposure of the pass area since the end of the Younger Dryas.

Acknowledgements

This study was supported by Swiss National Science Foundation Grant No.200020-118038 and 200020-118032/2 to C. Schlüchter and by AGH University of Science and Technology statutory grant No. 11.140.560 to J. Zasadni. We thank A. Süsli, D. Niederer and U. Menet for their support at the *in situ* ^{14}C extraction system and the tandem crew for AMS measurements. We sincerely thank N. Lifton for many valuable discussions. A critical review by B. Goehring helped improve this manuscript.

Editorial handling by: T. Jull

References

Alley, R.B., 2000. Ice-core evidence of abrupt climate changes. Proceedings of the National Academy of Sciences of the United States of America (PNAS) 97, 1331–1334.

Ammann, B., Lotter, A.F., Eicher, U., Gaillard, M.-J., Wohlfarth, B., Haeberli, W., Lister, G., Maisch, M., Niessen, F., Schlüchter, C., 1994. The Würmian Late-glacial in lowland Switzerland. Journal of Quaternary Science 9, 119–125.

Auer, M., 2003. Regionalisierung von Schneeparametern. In: Eine Methode zur Darstellung von Schneeparametern im Relief. Publikation Gewässerkunde, p. 304.

Balco, G., 2009. ^{26}Al–^{10}Be Exposure Age/Erosion Rate Calculators: Update from v. 2.1 to v.2.2. CRONUS-Earth Online Calculator Website.

Balco, G., Stone, J.O., Lifton, N.A., Dunai, T.J., 2008. A complete and easily accessible means of calculating surface exposure ages or erosion rates from ^{10}Be and ^{26}Al measurements. Quaternary Geochronology 3, 174–195.

Balco, G., Briner, J., Finkel, R.C., Rayburn, J.A., Ridge, J.C., Schaefer, J.M., 2009. Regional beryllium-10 production rate calibration for late-glacial northeastern North America. Quaternary Geochronology 4, 93–107.

Ballantyne, C.K., 1990. The Late Quaternary glacial history of the Trotternish Escarpment, Isle of Skae, Scotland, and its implications for ice-sheet reconstruction. Proceedings of the Geologists' Association 101, 171–186.

Benn, D.J., Evans, D.J.A., 2010. Glaciers & Glaciation. Hodder Education Publishers, London, p. 816.

Björck, S., Walker, M.J.C., Cwynar, L.C., Johnsen, S., Knudsen, K.-L., Lowe, J.J., Wohlfarth, B., INTIMATE Members, 1998. An event stratigraphy for the Last Termination in the North Atlantic region based on the Greenland ice-core record: a proposal by the INTIMATE group. Journal of Quaternary Science 13, 283–292.

Böhlert, R., Egli, M., Maisch, M., Brandová, D., Ivy-Ochs, S., Kubik, P.W., Haeberli, W., 2011. Application of a combination of dating techniques to reconstruct the

Lateglacial and early Holocene landscape history of the Albula region (eastern Switzerland). Geomorphology 127, 1–13.
Bortenschlager, S., 1984. Beiträge zur Vegetationsgeschichte Tirols I. Inneres Ötztal und unteres Inntal.
Briner, J.P., Young, N.E., Goehring, B.M., Schaefer, J.M., 2012. Constraining Holocene ^{10}Be production rates in Greenland. Journal of Quaternary Science 27, 2–6.
Chmeleff, J., von Blanckenburg, F., Kossert, K., Jakob, D., 2010. Determination of the ^{10}Be half-life by multi-collector ICP-MS and liquid scintillation counting. Nuclear Instruments and Methods in Physics Research B 268, 192–199.
Davis, B.A.S., Brewer, S., Stevenson, A.C., Guiot, J., Contributors, Data, 2003. The temperature of Europe during the Holocene reconstructed from pollen data. Quaternary Science Reviews 22, 1701–1716.
Debon, F., Lemmet, M., 1999. Evolution of Mg/Fe ratios in the late Variscan plutonic rocks from the external crystalline massifs of the Alps (France, Italy, Switzerland). Journal of Petrology 40, 1151–1185.
Draxler, I., 1977. Pollenanalytische Untersuchung von Mooren zur spät- und postglazialen Vegetationsgeschichte im Einzugsgebiet der Traun. Jahrbuch der Geologischen Bundesanstalt Wien 120, 131–163.
Dugan, B., 2008. New Production Rate Estimates for in Situ Cosmogenic 14C from Lake Bonneville, Utah, and Northwestern Scotland. Master thesis, University of Arizona.
Dühnfort, M., Anderson, R.S., Ward, D., Stock, G.M., 2010. Bedrock fracture control of glacial erosion processes and rates. Geology 38, 423–426.
Dunne, J., Elmore, D., Muzikar, P., 1999. Scaling factors for the rates of production of cosmogenic nuclides for geometric shielding and attenuation at depth on sloped surfaces. Geomorphology 27, 3–11.
Fabel, D., Stoeven, A.P., Harbor, J., Kleman, J., Elmore, D., Fink, D., 2002. Landscape preservation under Fennoscandian ice sheets determined from in situ produced ^{10}Be and ^{26}Al. Earth and Planetary Science Letters 201, 397–406.
Fabel, D., Harbor, J., Dahms, D., James, A., Elmore, D., Horn, L., Daley, K., Steele, C., 2004. Spatial patterns of glacial erosion at a valley scale derived from terrestrial cosmogenic ^{10}Be and ^{26}Al concentrations in rock. Association of American Geographers Annals 94, 241–255.
Federici, P.R., Granger, D.E., Pappalardo, M., Ribolini, A., Spagnolo, M., Cyr, A.J., 2007. Exposure age dating and Equilibrium Line Altitude reconstruction of an Egesen moraine in the Maritime Alps, Italy. Boreas 37, 245–253.
Federici, P.R., Granger, D.E., Ribolini, A., Spagnolo, M., Pappalardo, M., Cyr, A.J., 2012. Last Glacial Maximum and the Gschnitz stadial in the Maritime Alps according to ^{10}Be cosmogenic dating. Boreas 41 (2), 277–291. http://dx.doi.org/10.1111/j.1502–3885.2011.00233.x.
Fenton, C.R., Hermanns, R.L., Blikra, L.H., Kubik, P.W., Bryant, C., Niedermann, S., Meixner, A., Goethals, M.M., 2011. Regional ^{10}Be production rate calibration for the past 12 ka deduced from the radiocarbon-dated Grøtlandsura and Russenes rock avalanches at 69° N, Norway. Quaternary Geochronology 6, 437–452.
Fliri, F., 1973. Beiträge zur Geschichte der alpinen Würmvereisung: Forschungen am Bänderton von Baumkirchen (Inntal, Nordtirol). Zeitschrift für Geomorphologie Neue Forschungen 16, 1–14.
Florineth, D., 1998. Surface geometry of the Last Glacial Maximum (LGM) in the southeastern Swiss Alps (Graubünden) and its paleoclimatological significance. Eiszeitalter und Gegenwart 48, 23–37.
Florineth, D., Schlüchter, C., 1998. Reconstructing the Last Glacial Maximum (LGM) ice surface geometry and flowlines in the Central Swiss Alps. Eclogae geologicae Helvetiae 91, 391–407.
Florineth, D., Schlüchter, C., 2000. Alpine evidence for atmospheric circulation patterns in Europe during the last glacial maximum. Quaternary Research 54, 295–308.
Fraedrich, R., 1979. Spät- und postglaziale Gletscherschwankungen in der Ferwallgruppe (Tirol/Vorarlberg). Düsseldorfer Geographische Schriften 12, 1–161.
Frauenfelder, R., Haeberli, W., Hoelzle, M., Maisch, M., 2001. Using relict rockglaciers in GIS-based modelling to reconstruct Younger Dryas permafrost distribution patterns in the Err-Julier area, Swiss Alps. Norsk Geografisk Tidsskrift – Norwegian Journal of Geography 55, 195–202.
Frey, M., Teichmüller, M., Teichmüller, R., Mullis, J., Künzi, B., Breitschmid, A., Gruner, U., Schwizer, B., 1980. Very low grade metamorphism in external parts of the Central Alps: Illite crystallinity, coal rank and fluid inclusion data. Eclogae geologicae Helvetiae 73, 173–203.
Geyh, M.A., Schreiner, A., 1984. 14C-Datierungen an Knochen- und Stosszahnfragmenten aus Würmeiszeitlichen Ablagerungen im westlichen Rheingletschergebiet (Baden-Württemberg). Eiszeitalter und Gegenwart 34, 155–161.
Glasser, N.F., Bennett, M.R., 2004. Glacial erosional landforms: origins and significance for palaeoglaciology. Progress in Physical Geography 28, 43–75.
Goehring, B.M., Lohne, Ø.S., Mangerud, J., Svendsen, J.I., Gyllencreutz, R., Schaefer, J., Finkel, R., 2011. Late Glacial and Holocene ^{10}Be production rates for western Norway. Journal of Quaternary Science. http://dx.doi.org/10.1002/jqs.1517.
Gosse, J.C., Phillips, F.M., 2001. Terrestrial in situ cosmogenic nuclides: theory and application. Quaternary Science Reviews 20, 1475–1560.
Hajdas, I., Ivy, S.D., Beer, J., Bonani, G., Imboden, D., Lotter, A.F., Sturm, M., Suter, M., 1993. AMS radiocarbon dating and varve chronology of Lake Soppensee: 6000 to 12000 ^{14}C years BP. Climate Dynamics 9, 107–116.
Hallet, B., Hunter, L., Bogen, J., 1996. Rates of erosion and sediment evacuation by glaciers: a review of field data and their implications. Global and Planetary Change 12, 213–235.
Heisinger, B., Lal, D., Jull, A.J.T., Kubik, P., Ivy-Ochs, S., Neumaier, S., Knie, K., Lazarev, V., Nolte, E., 2002a. Production of selected cosmogenic radionuclides by muons: 1. Fast muons. Earth and Planetary Science Letters 200, 345–355.
Heisinger, B., Lal, D., Jull, A.J.T., Kubik, P., Ivy-Ochs, S., Knie, K., Nolte, E., 2002b. Production of selected cosmogenic radionuclides by muons: 2. Capture of negative muons. Earth and Planetary Science Letters 200, 357–369.
Heuberger, H., 1966. Gletschergeschichtliche Untersuchungen in den Zentralalpen zwischen Sellrain und Ötztal. Wissenschaftliche Alpenvereinshefte 20, 126.
Hippe, K., Kober, F., Baur, H., Ruff, M., Wacker, L., Wieler, R., 2009. The current performance of the *in situ* ^{14}C extraction line at ETH. Quaternary Geochronology 4, 493–500.
Hippe, K., Kober, F., Wacker, L., Fahrni, S.M., Ivy-Ochs, S., Akçar, N., Schlüchter, C., Wieler, R., 2013. An update on *in situ* cosmogenic ^{14}C analysis at ETH Zürich. Nuclear Instruments and Methods in Physics Research B 294, 81–86.
Hormes, A., Müller, B.U., Schlüchter, C., 2001. The Alps with little ice: evidence for eight Holocene phases of reduced glacier extent in the Central Swiss Alps. The Holocene 11, 255–265.
Hormes, A., Ivy-Ochs, S., Kubik, P.W., Ferreli, L., Michetti, A.M., 2008. ^{10}Be exposure ages of a rock avalanche and a late glacial moraine in Alta Valtellina, Italian Alps. Quaternary International 190, 136–145.
Ivy-Ochs, S., 1996. The Dating of Rock Surfaces Using in Situ Produced ^{10}Be, ^{26}Al and ^{36}Cl, with Examples from Antarctica and the Swiss Alps. Ph.D. thesis, ETH Zürich.
Ivy-Ochs, S., Schlüchter, C., Kubik, P.W., Beer, J., Kerschner, H., 1996. The exposure age of an Egesen moraine at Julier Pass measured with the cosmogenic radionuclides ^{10}Be, ^{26}Al and ^{36}Cl. Eclogae geologicae Helvetiae 89, 1049–1063.
Ivy-Ochs, S., Schlüchter, C., Kubik, P.W., Denton, G.H., 1999. Moraine exposure dates imply synchronous Younger Dryas glacier advances in the European Alps and in the Southern Alps of New Zealand. Geografiska Annaler 81, 313–323.
Ivy-Ochs, S., Schäfer, J., Kubik, P.W., Synal, H.-A., Schlüchter, C., 2004. Timing of deglaciation on the northern Alpine foreland (Switzerland). Eclogae geologicae Helvetiae 97, 47–55.
Ivy-Ochs, S., Kerschner, H., Kubik, P.W., Schlüchter, C., 2006a. Glacier response in the European Alps to Heinrich Event 1 cooling: the Gschnitz stadial. Journal of Quaternary Science 21, 115–130.
Ivy-Ochs, S., Kerschner, H., Reuther, A., Maisch, M., Sailer, R., Schaefer, J., Kubik, P.W., Synal, H., Schlüchter, C., 2006b. The timing of glacier advances in the northern European Alps based on surface exposure dating with cosmogenic ^{10}Be, ^{26}Al, ^{36}Cl, and ^{21}Ne. In: Siame, L.L., Bourlès, D.L., Brown, E.T. (Eds.), In Situ – Produced Cosmogenic Nuclides and Quantification of Geological Processes. Geological Society of America Special Paper, vol. 415, pp. 43–60.
Ivy-Ochs, S., Kerschner, H., Schlüchter, C., 2007. Cosmogenic nuclides and the dating of Lateglacial and Early Holocene glacier variations: the Alpine perspective. Quaternary International 164–165, 53–63.
Ivy-Ochs, S., Kerschner, H., Reuther, A., Preusser, F., Heine, K., Maisch, M., Kubik, P.W., Schlüchter, C., 2008. Chronology of the last glacial cycle in the European Alps. Journal of Quaternary Science 23, 559–573.
Ivy-Ochs, S., Kerschner, H., Maisch, M., Christl, M., Kubik, P.W., Schlüchter, C., 2009. Latest Pleistocene and Holocene glacier variations in the European Alps. Quaternary Science Reviews 28, 2137–2149.
Joerin, U.E., Stocker, T.F., Schlüchter, C., 2006. Multicentury glacier fluctuations in the Swiss Alps during the Holocene. The Holocene 16, 697–704.
Keller, O., Krayss, E., 1987. Die hochwürmzeitlichen Rückzugsphasen des Rhein-Vorlandgletschers und der erste alpine Eisrandkomplex im Spätglazial. Geographica Helvetica 42, 169–178.
Keller, O., Krayss, E., 2005. Der Rhein-Linth-Gletscher im letzten Hochglazial, 2. Teil: Datierung und Modelle der Rhein-Linth-Vergletscherung. Klima-Rekonstruktionen. Vierteljahresschrift der Naturforschenden Gesellschaft Zürich 150, 69–85.
Kelly, M.A., Buoncristiani, J.-F., Schlüchter, F., 2004a. A reconstruction of the last glacial maximum (LGM) ice-surface geometry in the western Swiss Alps and contiguous Alpine regions in Italy and France. Eclogae geologicae Helvetiae 97, 57–75.
Kelly, M.A., Kubik, P.W., von Blanckenburg, F., Schlüchter, C., 2004b. Surface exposure dating of the Great Aletsch Glacier Egesen moraine system, western Swiss Alps, using the cosmogenic nuclide ^{10}Be. Journal of Quaternary Science 19, 431–441.
Kelly, M.A., Ivy-Ochs, S., Kubik, P.W., von Blanckenburg, F., Schlüchter, C., 2006. Chronology of deglaciation based on ^{10}Be dates of glacial erosional features in the Grimsel Pass region, central Swiss Alps. Boreas 35, 634–643.
Kerschner, H., 1986. Zum Sendersstadium im Spätglazial der nördlichen Stubaier Alpen, Tirol. Zeitschrift für Geomorphologie Supplementband 61, 65–76.
Kerschner, H., 2005. Glacier–climate models as palaeoclimatic information sources: examples from the Alpine Younger Dryas period. In: Huber, U., Bugmann, H.K.M., Reasoner, M. (Eds.), Global Change and Mountain Regions. Springer, Dordrecht, pp. 73–81.
Kerschner, H., 2009. Gletscher und Klima im Alpinen Spätglazial und frühen Holozän. In: Schmidt, R., Matulla, C., Psenner, R. (Eds.), Klimawandel in Österreich. Die letzten 20.000 Jahre und ein Blick voraus. Alpine Space – Man & Environment, vol. 6. Innsbruck University Press, pp. 5–26.
Kerschner, H., Berktold, E., 1982. Spätglaziale Gletscherstände und Schuttformen im Senderstal, nördliche Stubaier Alpen, Tirol. Zeitschrift für Gletscherkunde und Glazialgeologie 17, 125–134.
Kerschner, H., Ivy-Ochs, S., 2008. Palaeoclimate from glaciers: examples from the Eastern Alps during the Alpine Lateglacial and early Holocene. Global and Planetary Change 60, 58–71.
Kerschner, H., Kaser, G., Sailer, R., 2000. Alpine Younger Dryas glaciers as palaeoprecipitation gauges. Annals of Glaciology 31, 80–84.

Kohl, C.P., Nishiizumi, K., 1992. Chemical isolation of quartz for measurement of in-situ-produced cosmogenic nuclides. Geochimica et Cosmochimica Acta 56, 3583–3587.
Korschinek, G., Bergmaier, A., Faestermann, T., Gerstmann, U.C., Knie, K., Rugel, G., Wallner, A., Dillmann, I., Dollinger, G., Lierse von Gostomski, C., Kossert, K., Maiti, M., Poutivtsev, M., Remmert, A., 2010. A new value for the half-life of ^{10}Be by heavy-ion elastic recoil detection and liquid scintillation counting. Nuclear Instruments and Methods in Physics Research B 268, 187–191.
Kubik, P.W., Christl, M., 2010. ^{10}Be and ^{26}Al measurements at the Zurich 6 MV Tandem AMS facility. Nuclear Instruments and Methods in Physics Research B 268, 880–883.
Labhart, T.P., 1999. Aarmassiv, Gotthardmassiv und Tavetscher Zwischenmassiv: Aufbau und Entstehungsgeschichte. In: Löw, S., Wyss, R. (Eds.), Vorerkundung und Prognose der Basistunnels am Gotthard und am Lötschberg. Balkema Rotterdam, pp. 31–43.
Labhart, T.P., 2009. Geologie der Schweiz. Ott Verlag, Thun, p. 211.
Lal, D., 1991. Cosmic ray labeling of erosion surfaces: in situ nuclide production rates and erosion models. Earth and Planetary Science Letters 104, 424–439.
Lifton, N.A., Jull, A.J.T., Quade, J., 2001. A new extraction technique and production rate estimate for in situ cosmogenic 14C in quartz. Geochimica et Cosmochimica Acta 65, 1953–1969.
Lifton, N.A., Caffee, M.W., Finkel, R., Schaefer, J.M., Stone, J., Goehring, B.M., Phillips, F., Oviatt, C.G., Rood, D.H., 2009. A New Estimate of the Spallogenic Production Rate of in Situ Cosmogenic ^{10}Be from Lake Bonneville Shoreline Features, Promontory Point. Utah. GSA Annual Meeting, Portland 18-21 Oct, paper no. 81-12.
Lister, G.S., 1988. A 15,000-Year isotopic record from lake Zürich of deglaciation and climatic change in Switzerland. Quaternary Research 29, 129–141.
Maisch, M., 1981. Glazialmorphologische und gletschergeschichtliche Untersuchungen im Gebiet zwischen Landwasser- und Albulatal (Kt. Graubünden, Schweiz). Physische Geographie 3, 215.
Maisch, M., 1982. Zur Gletscher- und Klimageschichte des alpinen Spätglazials. Geographica Helvetica 37, 93–104.
Maisch, M., 1987. Zur Gletschergeschichte des alpinen Spätglazials: Analyse und Interpretation von Schneegrenzdaten. Geographica Helvitica 42, 63–71.
Maisch, M., Wipf, A., Denneler, B., Battaglia, J., Benz, C., 1999. Die Gletscher der Schweizer Alpen. Gletscherhochstand 1850, Aktuelle Vergletscherung, Gletscherschwund-Szenarien. vdf Hochschulverlag ETH Zürich, p. 373.
Masarik, J., Frank, M., Schäfer, J.M., Wieler, R., 2001. Correction of in situ cosmogenic nuclide production rates for geomagnetic field intensity variations during the past 800,000 years. Geochimica et Cosmochimica Acta 65, 2995–3003.
Miller, G.H., Briner, J.P., Lifton, N.A., Finkel, R.C., 2006. Limited ice-sheet erosion and complex exposure histories derived from in situ cosmogenic ^{10}Be, ^{26}Al, and ^{14}C on Baffin Island, Arctic Canada. Quaternary Geochronology 1, 74–85.
Nesje, A., Dahl, S.O., Valen, V., Øvstedal, J., 1992. Quaternary erosion in the Sognefjord drainage basin, western Norway. Geomorphology 5, 511–520.
Oerlemans, J., 2001. Glaciers and Climate Change. A.A. Balkema Publishers, p. 148.
Oerlemans, J., Anderson, B., Hubbard, A., Huybrechts, P., Jóhannesson, T., Knap, W.H., Schmeits, M., Stroeven, A.P., van de Wal, R.S.W., Wallinga, J., Zuo, Z., 1998. Modelling the response of glaciers to climate warming. Climate Dynamics 14, 267–274.
Patzelt, G., 1972. Die spätglazialen Stadien und postglazialen Schwankungen von Ostalpengletschern. Berichte der Deutschen Botanischen Gesellschaft 85, 47–57.
Penck, A., Brückner, E., 1901/1909. Die Alpen im Eiszeitalter. Tauchitz, Leipzig, p. 1199.
Preusser, F., 2004. Towards a chronology of the Late Pleistocene in the northern Alpine Foreland. Boreas 33, 195–210.
Preusser, F., Graf, H.R., Keller, O., Krayss, E., Schlüchter, C., 2011. Quaternary glaciation history of northern Switzerland. Eiszeitalter und Gegenwart 60, 282–305.
Rasmussen, S.O., Andersen, K.K., Svensson, A.M., Steffensen, J.P., Vinther, B.M., Clausen, H.B., Siggaard-Andersen, M.-L., Johnsen, S.J., Larsen, L.B., Dahl-Jensen, D., Bigler, M., Röthlisberger, R., Fischer, H., Goto-Azuma, K., Hansson, M.E., Ruth, U., 2006. A new Greenland ice core chronology for the last glacial termination. Journal of Geophysical Research 111. http://dx.doi.org/10.1029/2005JD006079.
Reitner, J.M., 2007. Glacial dynamics at the beginning of termination I in the Eastern Alps and their stratigraphic implications. Quaternary International 164-165, 64–84.
Renner, F., 1982. Beiträge zur Gletschergeschichte des Gotthardgebietes und dendroklimatologische Analysen an fossilen Hölzern. Physische Geographie 8, 180.
Reuther, A.U., Fiebig, M., Ivy-Ochs, S., Kubik, P.W., Reitner, J.M., Jerz, H., Heine, K., 2011. Deglaciation of a large piedmont lobe glacier in comparison with a small mountain glacier – new insight form surface exposure dating. Two studies from SE Germany. Eiszeitalter und Gegenwart 60, 248–269.
Riihimaki, C.A., MacGregor, K.R., Anderson, R.S., Anderson, S.P., Loso, M.G., 2005. Sediment evacuation and glacial erosion rates at a small alpine glacier. Journal of Geophysical Research 110. http://dx.doi.org/10.1029/2004JF000189.
Ruff, M., Wacker, L., Gäggeler, H.W., Suter, M., Synal, H.-A., Szidat, S., 2007. A gas ion source for radiocarbon measurements at 200 kV. Radiocarbon 49, 790–794.
Schildgen, T.F., Phillips, W.M., Purves, R.S., 2005. Simulation of snow shielding corrections for cosmogenic nuclide surface exposure studies. Geomorphology 64, 67–85.
Schlüchter, C., 1988. A non-classical summary of the Quaternary stratigraphy in the Northern Alpine Foreland of Switzerland. Bulletin de la Société Neuchâteloise de Géographie 32, 143–157.
Schlüchter, C., 2004. The Swiss glacial record – a schematic summary. In: Ehlers, J., Gibbard, P.L. (Eds.), 2004. Quaternary Glaciations – Extent and Chronology, Part I: Europe. Developments in Quaternary Science, vol. 2a. Elsevier, Amsterdam, pp. 413–418.
Schlüchter, C., Röthlisberger, C., 1995. 100 000 Jahre Gletschergeschichte. In: Gletscher im ständigen Wandel. vdf-Hochschulverlag AG an der ETH Zürich, pp. 47–63.
Schmidt, R., Weckström, K., Lauterbach, S., Tessadri, R., Huber, K., 2011. North Atlantic climate impact on early late-glacial climate oscillations in the south-eastern Alps inferred from a multi-proxy lake sediment record. Journal of Quaternary Science. http://dx.doi.org/10.1002/jqs.1505.
Sergeev, S.A., Meier, M., Steiger, R.H., 1995. Improving the resolution of single-grain U/Pb dating by use of zircon extracted from feldspar: application to the Variscan magmatic cycle in the central Alps. Earth and Planetary Science Letters 134, 37–51.
Small, R.J., 1987. Moraine sediments budgets. In: Gurnell, A.M., Clarck, M.J. (Eds.), Glaciofluvial Sediment Transfer: an Alpine Perspective. John Wiley, Chichester, pp. 165–197.
Stone, J.O., 2000. Air pressure and cosmogenic isotope production. Journal of Geophysical Research 105, 23753–23759.
Stroeven, A.P., Fabel, D., Harbor, J., Hättestrand, C., Kleman, J., 2002. Quantifying the erosional impact of the Fennoscandian ice sheet in the Torneträsk-Narvik corridor, northern Sweden, based on cosmogenic radionuclide data. Geografiska Annaler 84, 275–287.
Synal, H.-A., Bonani, M., Döbeli, M., Ender, R.M., Gartenmann, P., Kubik, P.W., Schnabel, C., Suter, M., 1997. Status report of the PSI/ETH AMS facility. Nuclear Instruments and Methods in Physics Research B 123, 62–68.
Synal, H.-A., Stocker, M., Suter, M., 2007. MICADAS: a new compact radiocarbon AMS system. Nuclear Instruments and Methods in Physics Research B 259, 7–13.
van Husen, D., 2000. Geological processes during the Quaternary. Mitteilungen der Österreichischen Geologischen Gesellschaft 92, 135–156.
van Husen, D., 2004. Quaternary glaciations in Austria. In: Ehlers, J., Gibbard, P.L. (Eds.), Quaternary Glaciations – Extent and Chronology, Part I: Europe. Developments in Quaternary Science, vol. 2a. Elsevier, Amsterdam, pp. 1–13.
van Husen, D., Reitner, J., 2011. An outline of the quaternary stratigraphy of Austria. Eiszeitalter und Gegenwart 60, 366–387.
Vescovi, E., Ravazzi, C., Arpenti, E., Finsinger, W., Pini, R., Valsecchi, V., Wick, L., Ammann, B., Tinner, W., 2007. Interactions between climate and vegetation during the Lateglacial period as recorded by lake and mire sediment archives in Northern Italy and Southern Switzerland. Quaternary Science Reviews 26, 1650–1669.
Wacker, L., Bonani, G., Friedrich, M., Hajdas, I., Kromer, B., Němec, M., Ruff, M., Suter, M., Synal, H.-A., Vockenhuber, C., 2010. MICADAS: routine and high-precision radiocarbon dating. Radiocarbon 52, 252–262.
Wessels, M., 1998. Natural environmental changes indicated by Late Glacial and Holocene sediments from Late Constance, Germany. Palaeogeography, Palaeoclimatology, Palaeoecology 140, 421–432.
Wohlfarth, B., Gaillard, M.-J., Haeberli, W., Kelts, K., 1994. Environment and climate in southwestern Switzerland during the last termination, 15–10 ka BP. Quaternary Science Reviews 13, 361–394.